JACS
JOURNAL OF THE AMERICAN CHEMICAL SOCIETY

ARTICLE

pubs.acs.org/JACS

Mechanism of Carbon−Halogen Bond Reductive Cleavage in Activated Alkyl Halide Initiators Relevant to Living Radical Polymerization: Theoretical and Experimental Study

Abdirisak A. Isse,[±] Armando Gennaro,*[,±] Ching Yeh Lin,[‡] Jennifer L. Hodgson,[‡] Michelle L. Coote,*[,‡] and Tamaz Guliashvili*[,§]

[±]Department of Chemical Sciences, University of Padova, Via Marzolo 1, 35131 Padova, Italy

[‡]ARC Centre of Excellence for Free-Radical Chemistry and Biotechnology, Research School of Chemistry, Australian National University, Canberra ACT 0200, Australia

[§]GE Power & Water, Water & Process Technologies, 4636 Somerton Road, Trevose, Pennsylvania 19053, United States

Supporting Information

ABSTRACT: The mechanism of reductive cleavage of model alkyl halides (methyl 2-bromoisobutyrate, methyl 2-bromopropionate, and 1-bromo-1-chloroethane), used as initiators in living radical polymerization (LRP), has been investigated in acetonitrile using both experimental and computational methods. Both theoretical and experimental investigations have revealed that dissociative electron transfer to these alkyl halides proceeds exclusively via a concerted rather than stepwise manner. The reductive cleavage of all three alkyl halides requires a substantial activation barrier stemming mainly from the breaking C−X bond. The activation step during single electron transfer LRP (SET-LRP) was originally proposed to proceed via formation and decomposition of $RX^{\bullet-}$ through an outer sphere electron transfer (OSET) process (Guliashvili, T.; Percec, V. *J. Polym. Sci., Part A: Polym. Chem.* **2007**, *45*, 1607). These radical anion intermediates were proposed to decompose via heterolytic rather than homolytic C−X bond dissociation. Here it is presented that injection of one electron into RX produces only a weakly associated charge-induced donor−acceptor type radical anion complex without any significant covalent σ type bond character between carbon-centered radical and associated anion leaving group. Therefore, neither homolytic nor heterolytic bond dissociation applies to the reductive cleavage of C−X in these alkyl halides inasmuch as a true radical anion does not form in the process. In addition, the whole mechanism of SET-LRP has to be revisited since it is based on presumed OSET involving intermediate $RX^{\bullet-}$, which is shown here to be nonexistent.

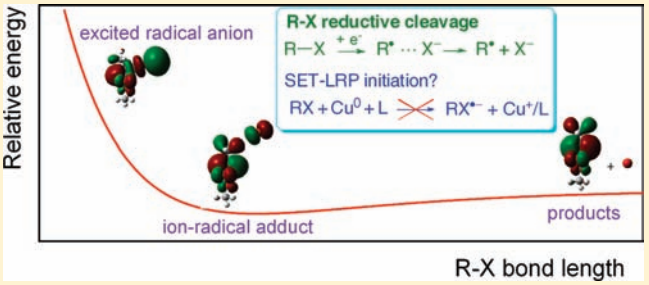

INTRODUCTION

Transition metal-mediated controlled/"living" radical polymerization (often called atom transfer radical polymerization or ATRP) is one of the widely used synthetic methodologies for the preparation of polymers with well-defined compositions, architectures, chain-end functionalities and predetermined molecular weight (MW), and low polydispersity index (PDI).[1−5] Mechanistically, ATRP is based on a transition metal complex-mediated fast equilibrium between dormant (unimeric or polymeric initiator: R−X; X = halogen or pseudohalogen) and active (radical or macroradical, R•) species. Homolytic cleavage of the C−X bond of dormant species is catalyzed by a lower oxidation state transition metal complex (activator = $Mt^{(z)}X_m$/L). The generated macroradical (R•) reacts with a higher oxidation state transition metal complex (deactivator = $Mt^{(z+1)}X_{m+1}$/L), forming dormant species and regenerating the activator (Scheme 1). The equilibrium shown in Scheme 1 is typically shifted toward dormant species ($k_{act} \ll k_{deact}$) so that the radical−radical termination reactions are diminished because of the persistent radical effect.[6] The controlled/"living" character of polymerization (control over MW, PDI, chain-end functionality, etc.) strongly depends on the K_{ATRP} value ($K_{ATRP} = k_{act}/k_{deact}$).[3,5]

The mechanism of activation of RX should be analyzed in the framework of dissociative electron transfer (DET) to C−X bonds in organic halides. Two reaction pathways are possible (Scheme 2) for the reductive cleavage of RX to R• and X^-.[7] These are a stepwise mechanism involving an intermediate radical anion, $RX^{\bullet-}$, which further decomposes to R• and X^-, and a concerted mechanism in which electron transfer and bond breaking occur in a single step. If R• has a dipole moment, it may interact with X^- to form an ion−radical adduct ($R^{\bullet}\cdots X^-$) in which the two fragments are held together by electrostatic interactions rather than a true covalent bond.[8,9] The interaction

Received: November 23, 2010
Published: February 07, 2011

Scheme 1. General Mechanism of ATRP (X = Cl, Br, I, SCN; L = nitrogen-, phosphorus-, C_p-based ligand; Mt = Cu, Ru, Fe, Os, Ni, etc.; z = 0, 1, 2, etc.; m = 0, 1, 2, etc.)

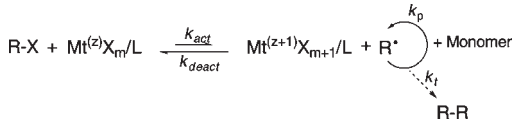

Scheme 2. General Reductive Cleavage Mechanism of Organic Halides

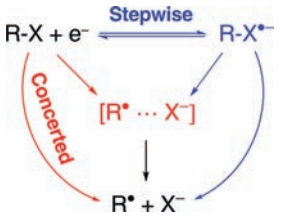

Scheme 3. Alternative Activation Pathways of R−X under ISET (blue) or OSET (red) Conditions for Cu^IX/L-Catalyzed Systems

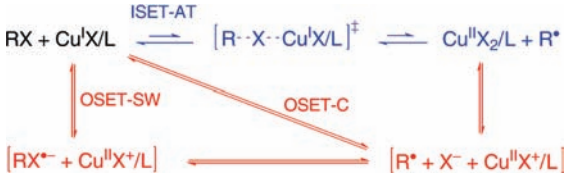

Scheme 4. Mechanism of Cu^0-Catalyzed Activation/Deactivation Proposed for SET-LRP

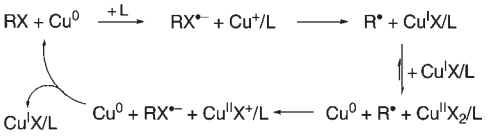

energy, D_p, depends on the dipole moment of $R^•$, charge density on X^- and the nature of the solvent.[9,10]

Dissociative electron transfer to a large number of aromatic and aliphatic halides has been studied both theoretically[11−14] and experimentally.[8−10,15,16] It is found that aromatic halides undergo a stepwise mechanism, whereas the concerted mechanism is the preferred reaction route for simple alkyl halides. Aromatic halides, ArX, possess low-lying π^* orbitals in which the incoming electron is first accommodated. Thus, depending on the chemical structure of ArX, radical anions with a wide range of lifetimes are formed. The decay of these radical anions is viewed as a shift of the electron from π^* to the σ^* molecular orbital of the C−X bond accompanied by rupture of the latter (intramolecular concerted DET).[17] Simple alkyl halides do not possess low-lying antibonding orbitals; in this case, the incoming electron ends in the σ^* orbital of the C−X bond, thus causing dissociation of the bond with electron injection. Benzyl halides were found to be in a borderline situation; unsubstituted benzyl and benzyl-type halides undergo concerted DET, whereas nitrobenzyl halides prefer a stepwise mechanism, the electron being initially localized in the nitro group.[15b] Other examples showing that reductive cleavage of aliphatic halides bearing π acceptors may follow a stepwise mechanism with the intermediate formation of radical anions have been reported.[18] Activated alkyl halides used as initiators in ATRP have unsaturated groups such as Ph, CN, and CO_2R, which can accommodate the incoming electron in a π^* orbital. Therefore, classification of their DET mechanism as either concerted or stepwise is not an easy task.

Since the copper-based catalytic systems are superior in ATRP, most mechanistic studies of activation and deactivation processes have been based on Cu^IX/L and $Cu^{II}X_2/L$ complexes.[19−25] Activation and deactivation during Cu^IX/L-mediated ATRP have been proposed to occur via atom transfer (AT) involving a bonded transition state in which the halogen atom acts as a bridge between R and Cu (Scheme 3).[3,19,26,27] Formally, this AT process can be viewed as an inner-sphere electron transfer (ISET) involving the concerted transfer of an electron and a halide ion, the first from the metal center to the dormant species and the second from RX to the metal. According to this formalism, the activation process involves a Cu^IX/L-catalyzed homolytic dissociation of a C−X bond. A possible alternative to ISET-AT is an outer-sphere electron transfer (OSET) between RX and Cu^IX/L leading to $R^•$, X^- and $Cu^{II}X^+/L$, followed by coupling of the halide ion with the metal center.[26] In outer-sphere electron transfer processes there is no bonded complex between the transition metal center and dormant species, and transfer of the electron and the halogen occur sequentially. Note that in the OSET mechanism bond breaking may either occur in a distinct step after electron transfer (OSET-SW) or be concerted with electron transfer (OSET-C).

In contrast to standard ATRP, the activation of dormant species (R−X) with zerovalent copper in the presence of chelating nitrogen-based ligands and polar media (dipolar aprotic or protic solvents) has been postulated to occur through an OSET mechanism involving the formation of radical anion intermediates.[28,29] The resulting Cu^I catalyst is then proposed to undergo spontaneous disproportionation to Cu^0 and Cu^{II}, the former undergoing further reaction with R−X and the latter with X^- (Scheme 4).[28] The polymerization process is thus catalyzed by Cu^0 rather than the conventional Cu^I complexes, the role of the latter being limited to the regeneration of the real activator. For this reason, Cu^0-mediated controlled radical polymerization processes have been classified separately from ATRP as single electron transfer living radical polymerization (SET-LRP).[28] However, the precise mechanism of activation during the SET-LRP process is still under debate.[14,30,31] The ISET process cannot be excluded during the activation step of SET-LRP (reaction of R−X with Cu^0), since the halide atom after activation binds Cu^I species within the transition metal coordination sphere.[3] This fact may serve as evidence that a halide bridge is formed with Cu^0 and dormant species R−X (a key requirement of ISET process). It should also be noted that Cu^0 catalysts have been used successfully in standard ATRP processes both for direct reaction and regeneration of Cu^I.[32]

A crucial point in the analysis of the activation mechanism of ATRP and SET-LRP is whether the reductive cleavage of RX follows an ISET or OSET pathway with the formation of an intermediate radical anion $RX^{•−}$. In particular, it has been claimed that mechanistically SET-LRP is distinguished from all other controlled/"living" radical polymerization techniques

dx.doi.org/10.1021/ja110538b | J. Am. Chem. Soc. 2011, 133, 6254–6264

(including ATRP, nitroxide-mediated polymerization (NMP), reversible addition−fragmentation chain transfer polymerization (RAFT), etc.) as being so far the only example where the activation of dormant species involves intermediate $RX^{\bullet -}$, which decomposes via "heterolytic" C−X bond dissociation.[31] However, neither the possibility of the OSET mechanism nor the mode of dissociation of C−X bond in the hypothesized radical anion has never been examined. It is the purpose of this work to examine in more detail the mechanism of dissociative electron transfer to some alkyl halides used as initiators in SET-LRP and ATRP. A combined theoretical and experimental investigation will be carried out on the dynamics and thermodynamics of ET to RX with the aim of establishing whether $RX^{\bullet -}$ is an intermediate or not. In addition, if it turns out that OSET does indeed occur to produce $RX^{\bullet -}$, the mechanism of bond dissociation in the radical anion will be examined in detail.

There is no doubt that the mechanism of initiation in transition metal-catalyzed LRP strictly relies on the mechanism of reductive cleavage of alkyl halides used as initiators. On the other hand, also the activation step of the dormant species during LRP involves the reductive cleavage of the terminal C−X bond. A clear understanding of the latter will enable a precise evaluation of some aspects of LRP mechanism, such as, for example, the role of OSET. Furthermore, careful analysis of the dynamics of dissociative electron transfer to RX will provide important activation-driving force relationships that may be utilized to predict whether a given catalyst may function as an OSET donor in ATRP and SET-LRP or not.

COMPUTATIONAL PROCEDURES

To study the radical anion decomposition process, we have calculated the orbitals, charges, and spin distributions for a series of neutral alkyl halides (R−X = $BrCH(CH_3)COOCH_3$, $BrC(CH_3)_2COOCH_3$, and $BrCH(CH_3)Cl$), chosen to model the unimeric dormant species, i.e., the corresponding alkyl bromides of methyl acrylate (MA), methyl methacrylate (MMA), and vinyl chloride (VC), respectively. We have then repeated the calculations for the corresponding vertically excited radical anions and for various structures along the minimum energy path for their decomposition into $R^{\bullet}$ and X^{-}.

All calculations were performed in Gaussian 03[33a] and/or GAMESS 2008.[33b] All orbital visualizations were carried out in MacMolPlot.[33c] As in our previous studies,[14] geometries were initially optimized at the B3-LYP/6-31+G(d) level of theory. For the nonstationary species along the R−X dissociation path, constrained optimizations were performed in which the R−X bond was frozen at the specified value. For the potential energy surface calculations (neutral molecule C-Br bond homolysis and reductive cleavage of alkyl halides) and determination of the activation barriers, improved calculations were performed using the multireference method MRMP2/6-31+G(d)//MCSCF/6-31+G(d) to ensure the high accuracy of the energy at elongated bond distance; solvent effects were modeled using the PCM-UAHF method.

Natural bond orbital (NBO) calculations were performed using the B3-LYP/6-311+G(3df,2p) wave function in the gas phase and in acetonitrile solution; solvent effects were modeled using the PCM-UAKS method. Mulliken population analysis was performed as recommended[34] using the smaller basis set B3-LYP/6-31+G(d) level of theory. The results from both procedures were in excellent agreement with one another except in the case of the vertically excited VC-Br radical anion. For this species, discriminating calculations were also performed using atoms-in-molecules (AIM) theory, with the results supporting the NBO analysis. Full results are provided in the Supporting Information, while for clarity only the NBO results are provided in the main paper. Charge and spin density calculations were performed using both restricted and unrestricted open-shell procedures, with both procedures giving almost identical results; the latter are provided in the Supporting Information. However, because of problems arising from spin contamination, the orbitals were plotted from the restricted open-shell calculations only.

EXPERIMENTAL SECTION

Materials. Acetonitrile (Carlo Erba, RS) was distilled over CaH_2 and stored under argon atmosphere. Tetraethylammonium tetrafluoroborate (Et_4NBF_4, Alfa Aesar, 99%) was recrystallized from ethanol and dried in a vacuum oven at 70 °C for 48 h. Methyl 2-bromopropionate (Aldrich, 98%), methyl 2-bromoisobutyrate (Aldrich, ≥99%) and 1-bromo-1-chloroethane (Alfa Aesar, 98%) were used as received.

Cyclic Voltammetry. Voltammetric measurements were carried out on a computer-controlled Autolab PGSTAT30 potentiostat (Eco-Chimie, Utrecht, The Netherlands). All experiments were carried out at 25 °C in a three-electrode cell system using a glassy carbon (GC) disk (3 mm diameter, Tokay GC20) as a working electrode. The counter-electrode and the reference electrode were a Pt ring and $Ag|AgI|I^-$ 0.1 M $n\text{-}Bu_4NI$ in dimethylformamide, respectively. All potentials are, however, reported versus the KCl-saturated aqueous calomel electrode (SCE). This has been done by calibrating during each experiment the $Ag|AgI|I^-$ reference electrode against the ferrocenium/ferrocene couple ($E^{o}_{Fc^+/Fc}$ = 0.391 V vs SCE in CH_3CN), which was used as an internal redox reference system, and converting the measured potentials to the SCE scale. Prior to each experiment the working electrode surface was cleaned by polishing with a 0.25-μm diamond paste, followed by ultrasonic rinsing in ethanol for 5 min.

RESULTS AND DISCUSSION

Table 1 shows the total charges and spin densities on R and X in the excited R−X radical anions, for R−X = $BrCH(CH_3)COOCH_3$ (MA-Br), $BrC(CH_3)_2COOCH_3$ (MMA-Br), and $BrCH(CH_3)Cl$ (VC-Br). These species were selected as model monomeric initiators, mimicking the Br terminated macroinitiators, used in the successful SET-LRP process of methyl acrylate, methyl methacrylate, and vinyl chloride monomers, respectively.[31] For each species, results are shown at various places along the minimum energy path for the dissociation of the radical anion, starting from the vertically excited species (i.e., the radical anion formed by injecting an electron into the neutral species without allowing for the geometry to relax). The calculations were performed both in the gas and solution phases. As we have noted previously,[14] in the gas phase this vertically excited radical anion decomposes into a weak complex between the alkyl radical and the halide ion ($R^{\bullet}\cdots X^{-}$), before it fully fragments into $R^{\bullet}$ and X^{-}. In contrast, formation of a stable complex could not be observed in solution; the radical anion dissociates fully. In either case, in the fully dissociated products, all of the −1 negative charge is borne on the halogen whereas all of the +1 spin density is borne on the alkyl radical.

To assist in the study of the mechanism, we also examined the relevant orbitals of the neutral alkyl halide and corresponding excited radical anions (ERAs). Figure 1 shows the lowest unoccupied molecular orbital (LUMO) for the three neutral alkyl halides studied; in each case this orbital clearly corresponds, as

Table 1. Computed Charge and Spin Distribution Data of Neutral Alkyl Halides and Their Radical Anions (RA) at Various Points along the Minimum Energy Path for Their Dissociation[a]

			gas-phase				solution-phase (acetonitrile)			
			charge		spin density		charge		spin density	
species		R−X bond length (Å)	on R	on X	on R	on X	on R	on X	on R	on X
MA-Br	neutral	1.992	−0.01	0.01	−	−	0.00	0.00	−	−
	ERA	1.992	−0.57	−0.43	0.56	0.44	−0.52	−0.48	0.56	0.44
	stable product	4.411	−0.11	−0.89	0.92	0.08	−0.04	−0.96	0.99	0.01
MMA-Br	neutral	2.017	0.00	0.00	−	−	0.01	−0.01	−	−
	ERA	2.017	−0.57	−0.43	0.57	0.43	−0.50	−0.50	0.55	0.45
	stable product	4.103	−0.07	−0.93	0.97	0.03	−0.03	−0.97	0.99	0.01
VC-Br	neutral	1.975	−0.03	0.03	−	−	−0.02	0.02	−	−
	ERA	1.975	−0.55	−0.45	0.55	0.45	−0.38	−0.62	0.42	0.58
	stable product	3.588	−0.03	−0.97	1.00	0.00	−0.02	−0.98	1.00	0.00

[a] Calculated on the basis of an NBO population analysis at the UB3-LYP/6-311+G(3df,2p)//UB3-LYP/6-31+G(d) level of theory. Solution-phase data in acetonitrile solvent were obtained using the PCM model at the same level of theory for gas-phase-optimized reaction species. ERA refers to the vertically excited radical anion. Stable product stands for the cleavage products with minimum energy, i.e., an ion−radical adduct in the gas phase and separated fragments in acetonitrile.

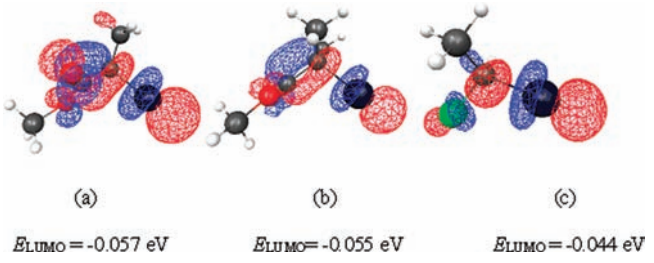

Figure 1. The shape and energy of LUMO of the neutral alkyl halides: (a) MA-Br, (b) MMA-Br, (c) VC-Br (calculated at ROB3-LYP/6-31+G(d) level of theory in the gas phase). The blue and red colors denote the opposite phases of the wave function.

expected, to the antibonding orbital of the R−X bond. Figure 2 shows the σ bonding orbital and σ antibonding orbital of the radical anion of methyl 2-bromopropionate (MA-Br) at various places along the reaction path for its dissociation. It should be noted that although the σ antibonding orbital always corresponds to the singly occupied molecular orbital (SOMO), the σ orbital does not always correspond to the second highest occupied molecular orbital (HOMO-1). It can be seen that as the bond distance increases, the energies of these two orbitals get closer and the σ orbital eventually becomes HOMO-1. In addition, during bond elongation the SOMO and the HOMO-1 molecular orbitals get localized onto the MA$^{\bullet}$ radical site and Br^{-} lone pair, respectively. Equivalent pictures for the other alkyl halide radical anions studied are provided in the Supporting Information.

Cleavage Mechanism. Activation of RX by Cu^{I} or Cu^{0} involves cleavage of the C−X bond, and the terms homolytic and heterolytic bond cleavage are sometimes used to distinguish different activation mechanisms. As shown in Scheme 2 (ISET-AT pathway), activation of RX to give R$^{\bullet}$ and $Cu^{II}X_2$/L in ATRP may be viewed as a Cu^{I}X/L-catalyzed homolytic cleavage of RX. In contrast, Percec[31] defined RX activation by Cu^{0} in SET-LRP as a heterolytic bond cleavage of RX to give R$^{\bullet}$ and Cu^{I}X/L. It would be interesting to examine the bond cleavage mode in the light of the computational results obtained in this study. In fact, from the results in Table 1 and Figures 1 and 2, a clear picture of the cleavage mechanism in alkyl halides emerges. When the neutral alkyl halide receives an electron, this electron initially populates the lowest unoccupied orbital of the alkyl halide, which (as seen in Figure 1) is the antibonding orbital of the R−X σ bond. Thus, in Figure 2, it is seen that the singly occupied orbital of the vertically excited radical anion closely resembles the antibonding orbital in the corresponding neutral species in Figure 1. By placing electron density in this antibonding orbital, it destabilizes the bond, ultimately leading to cleavage. By following the changes to the shape of this singly occupied orbital as the excited radical anion starts to dissociate, we note that this SOMO, initially distributed over both R and X starts to localize on R. At the same time, the bonding pair of electrons from the R−X σ bond moves in the opposite direction toward X, forming one of its lone pair orbitals. These qualitative changes in the orbital shapes are mirrored by the quantitative changes to the charge and spin densities (Table 1). Initially, the +1 spin density and −1 charge density are distributed more or less equally over R and X, reflecting the distribution of the antibonding orbital of the R−X bond. However, over the course of the dissociation, the spin density grows on R and the charge grows on X so that by the time the ion−radical adduct is formed (in the gas phase) it is essentially composed of two interacting fragments (referred to in the literature as a "sticky pair"[8,9]) held together by a very weak ion−dipole interaction. This adduct is characterized by most (∼80 −100%) of the total spin density being on R, most (∼80−100%) of the total negative charge on X, and a large separation between R$^{\bullet}$ and X^{-} (∼4 Å). It is also important to mention that the VC-Br neutral molecule LUMO energy (Figure 1) is higher than the corresponding LUMO energies of the more "activated" MA-Br and MMA-Br. This observation partially explains why it is difficult to activate the Br-terminated poly(vinyl chloride) macroinitiator (PVC-Br) under the proposed OSET process.[28]

In general, the cleavage of a radical anion into the radical and anion can be classified as homolytic (Scheme 5a) or heterolytic (Scheme 5b).[35] The homolytic C−X bond cleavage occurs when the most of the negative charge of the radical anion is mainly localized on the anion-leaving group (X^{-}). In this case *no* charge

dx.doi.org/10.1021/ja110538b |*J. Am. Chem. Soc.* 2011, 133, 6254–6264

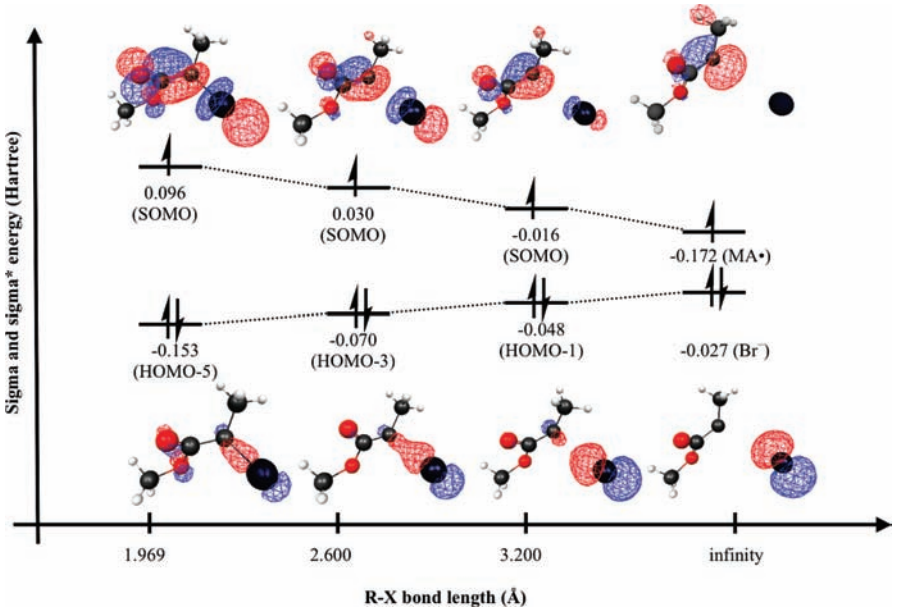

Figure 2. Changes to the energy and shape of the σ bonding and antibonding orbitals during the decomposition of the ion−radical adduct of methyl 2-bromopropionate (MA-Br). Orbitals and electronic energies were calculated at ROB3-LYP/6-31+G(d) in the gas phase; the blue and red colors denote the opposite phases of the wave function.

Scheme 5. Mechanism of (a) Homolytic and (b) Heterolytic C−X Bond Dissociation in Radical Anions

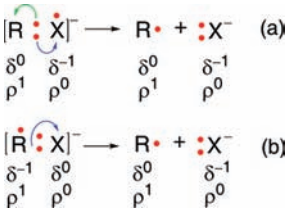

transfer occurs during the dissociation and the C−X σ bond of the radical anion must cleave homolytically, thus allowing the X group to leave as an anion (X^-). The other electron of the original C−X σ bond becomes the unpaired 2p electron on $C^\bullet$. However, if the negative charge is not localized on the X^- leaving group, the C−X bond dissociates via a heterolytic pathway in which the excess electron shifts from the breaking C−X σ bond to X^-. This second case fits very well the mechanism proposed for DET to aromatic halides, whereby the incoming electron is first accommodated in a π^* orbital and is later shifted to the σ^* orbital of the C−X bond in a concerted intramolecular dissociative electron transfer.[17]

If we analyze our present results for alkyl halides in terms of these definitions, we first note that these classifications refer to the cleavage of a *covalent* bond. According to our computational results and also experimental data (see later), injection of an electron into R−X does not produce a radical anion. Calculations show that an ion−dipole adduct is formed in the gas phase, dissociation of the C−X σ bond being concerted with electron injection. Since there is no covalent bond in this adduct, the homolytic vs heterolytic nomenclature defined above for true radical anions cannot be applied to the reductive cleavage of the examined alkyl halides. The concerted dissociative electron transfer to these alkyl halides can be schematically represented as shown in Scheme 6. The incoming electron goes to the

Scheme 6. Schematic Representation of the Reductive Cleavage Mechanism of Alkyl Halides

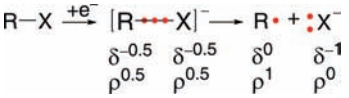

σ antibonding of the R−X bond, resulting in a roughly equal repartition of both the negative charge and spin density between the carbon and halogen atoms.

In living radical polymerization the terms homolytic and heterolytic R−X bond dissociation bear a more profound significance than what the definitions illustrated in Scheme 5 give. They were coined to indicate the mechanism of activation of RX by Cu^I and Cu^0. The commonly accepted mechanism of RX activation in Cu^I-catalyzed ATRP involves a transfer of a halogen atom from RX to Cu^IX/L or alternatively an ISET in which the halogen atom serves as a bridge between the metal and the alkyl group. Since in this case there is no charge transfer between R and X during the course of the reaction, the process may in principle be referred to as a homolytic dissociation. On the other hand, the mechanism proposed for SET-LRP involves an OSET from Cu^0 to RX with the intermediate formation of $RX^{\bullet -}$. However, the results reported in this paper unequivocally rule out the possibility of $RX^{\bullet -}$ formation. Thus, even if Cu^0-catalyzed SET-LRP could be initiated by electron transfer, DET to RX should follow a concerted mechanism, which means that C−X bond dissociation cannot be classified as either homolytic or heterolytic. Therefore, the term heterolytic dissociation used to indicate the mechanism of SET-LRP appears to be inappropriate.

Kinetics and Thermodynamics of the Reductive Cleavage of RX. Comparison between Experimental and Theoretical Results. In order to determine some relevant kinetic and thermodynamic parameters of the DET to MA-Br, MMA-Br, and VC-Br, combined experimental and theoretical methods were applied. For experimental studies, cyclic voltammetry (CV)

dx.doi.org/10.1021/ja110538b |*J. Am. Chem. Soc.* 2011, 133, 6254–6264

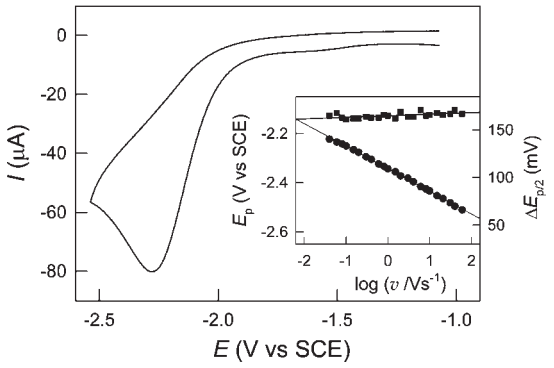

Figure 3. Cyclic voltammetry of 1.2 mM 1-bromo-1-chloroethane in CH_3CN + 0.1 M Et_4NBF_4, recorded at a glassy carbon electrode at v = 0.2 V s^{-1}. The inset shows dependence of E_p (●) and $\Delta E_{p/2}$ (■) on scan rate.

Table 2. Electrochemical Data for the Dissociative ET to RBr and Some Parameters Required for the Analysis of the Process

RBr	E_p[a], V vs SCE	α[b]	D, cm^2 s^{-1}	Z, cm s^{-1}	a_{RBr}, Å
MA-Br	−1.77	0.28	3.0×10^{-5}	4.86×10^3	3.54
MMA-Br	−1.78	0.27	2.8×10^{-5}	4.67×10^3	3.72
VC-Br	−2.28	0.31	3.5×10^{-5}	5.24×10^3	3.24

[a] At v = 0.2 V s^{-1}. [b] Average of the values from E_p vs log v and $\Delta E_{p/2}$.

was used to assess some relevant kinetic and thermodynamic parameters of the reductive cleavage of the aforementioned alkyl halides. In cyclic voltammetry (CV) performed in CH_3CN + 0.1 M Et_4NBF_4, all three alkyl bromides show a single broad, irreversible reduction peak. An example of the CV reduction of RBr is given in Figure 3, whereas the peak potentials measured at v = 0.2 V s^{-1} are reported in Table 2 for all three compounds.

Owing to the greater electron-withdrawing ability of a CO_2CH_3 group with respect to Cl,[36] the two ester derivatives, which have similar reduction potentials, are about 0.5 V more easily reducible than VC-Br. This result confirms the greater difficulty to activate PVC-Br with Cu^I complexes as compared with more activated alkyl halides such as MMA-Br and MA-Br[28,37] The single irreversible peak observed for these compounds is typical of the electrochemical reduction of many alkyl halides, which are known to undergo dissociative electron transfer (ET).[8,9,15] The radical $R^•$ ensuing from the reductive cleavage of RBr is often much easier to reduce than the starting molecule.[38] We thus expect an overall $2e^-$ process according to the following equations:

$$RBr + e^- \rightarrow R^• + Br^- \quad (1)$$

$$R^• + e^- \rightleftarrows R^- \quad (2)$$

The reduction process may be complicated by father−son reactions between the electrogenerated carbanion and the starting molecule. In particular, if the activated alkyl halide bears α-hydrogen atoms as, for example, in XCH_2CN, $XCH_2CO_2CH_3$, and $CH_3CHXCO_2CH_3$, the starting compound may act as a proton donor toward the carbanion R^-. The effect of father−son reactions is to subtract part of the starting substrate to the overall reduction process, resulting in CV responses with currents smaller than expected for a $2e^-$ process.[39] These undesired reactions can be easily suppressed by adding a proton donor stronger than RX. We checked the occurrence of father−son reactions in the electrochemical reduction of the three alkyl halides under investigation, but only $CH_3CHXCO_2CH_3$ has shown to be capable of reacting with the electrogenerated R^-. To avoid father−son reactions, all CV investigations on this compound were carried out in the presence of an equimolar amount of benzamide, which was found to react with R^- faster than MA-Br.

Voltammetric analysis of the peak characteristics can provide important information on the mechanism of the dissociative ET. In particular, the transfer coefficient (α), which is related to the intrinsic barrier ($\Delta G_0^‡$) can be used to discriminate between concerted and stepwise dissociative ET processes. In fact, concerted dissociative ET processes are characterized by α values significantly lower than 0.5,[8,9,15] whereas stepwise mechanisms often show an α value close to or higher than 0.5.[16] Experimentally, α can be easily determined by voltammetric analysis of the reduction process. The peak potential and the half-peak width ($\Delta E_{p/2} = E_{p/2} - E_p$) of an electrode process under kinetic control of the ET are given by[40]

$$E_p = E^{o\prime} - \frac{RT}{\alpha F}\left[0.78 + \ln\left(\frac{D^{1/2}}{k^\circ}\right) + \ln\left(\frac{\alpha F v}{RT}\right)^{1/2}\right] \quad (3)$$

$$\Delta E_{p/2} = E_{p/2} - E_p = \frac{1.857RT}{\alpha F} \quad (4)$$

where k° is the standard rate constant of electron transfer (ET), D is the diffusion coefficient of the electroactive species, F is the Faraday constant, and v is the scan rate. Provided that α remains constant in the investigated potential range, which is the case of most alkyl halides,[8,15] E_p should vary linearly with log v, while $\Delta E_{p/2}$ is expected to be independent of v. This is exactly what is found for all three alkyl bromides. An example of the dependence of E_p and $\Delta E_{p/2}$ on the scan rate is shown in the insert of Figure 3. Equations 3 and 4 were used to determine α for each compound, and the average of values obtained from the two methods, which give practically the same values, are reported in Table 2. The smallness of the transfer coefficient (α is near 0.3) is a clear indication that the dissociative ET follows a concerted mechanism, which confirms the results of the theoretical calculations.

We may now analyze the kinetics of the ET according to the dissociative ET theory.[41] The original version of this theory gives the following relationship between the activation free energy, $\Delta G^‡$, and the standard free energy of the reaction:[41b]

$$\Delta G^‡ = \Delta G_0^‡\left(1 + \frac{\Delta G^\circ}{4\Delta G_0^‡}\right)^2 = \frac{D_{RX}+\lambda_o}{4}\left(1+\frac{\Delta G^\circ}{D_{RX}+\lambda_o}\right)^2 \quad (5)$$

in which D_{RX} is the R−X bond dissociation energy, λ_o is the solvent reorganization energy, and $\Delta G_0^‡$ is the intrinsic barrier, that is, the activation free energy at zero driving force. To apply eq 5, we need to extract a set of $\Delta G^‡$ and ΔG^o values from the experimental data. We will use again the peak characteristics. The activation free energy at the peak potential, $\Delta G_p^‡$, can be calculated from eq 6:[42]

$$\Delta G_p^‡ = \frac{RT}{F}\left[\ln\left(Z^{el}\sqrt{\frac{RT}{\alpha F D v}}\right) - 0.78\right] \quad (6)$$

dx.doi.org/10.1021/ja110538b | J. Am. Chem. Soc. 2011, 133, 6254–6264

Table 3. Kinetic and Thermodynamic Parameters of Relevance in the Analysis of Dissociative ET to Some Alkyl Bromides in CH_3CN

RBr	D_{RX},[a] kJ mol^{-1}	$\Delta_{BD}G^o$,[a] kJ mol^{-1}	$E^o_{X^\bullet/X^-}$[b] V vs SCE	$E^o_{RX/R^\bullet+X^-}$[b] V vs SCE	a, Å	λ_o, kJ mol^{-1}	$\Delta G_0^{\ddagger}$(pred)[c], kJ mol^{-1}	$\Delta G_0^{\ddagger}$(exptl)[d], kJ mol^{-1}	D_p, kJ mol^{-1}
MA-Br	262.9	220	1.60	−0.68	2.83	102.2	91.3	73.8	4.05
MMA-Br	258.4	216	1.60	−0.64	2.89	100.3	89.7	77.1	2.22
VC-Br	276.9	234	1.60	−0.83	2.74	105.8	95.7	86.2	1.25

[a] Taken from ref 14. [b] Taken from ref 44. [c] Value predicted according to the original version of dissociative electron transfer theory: $\Delta G_0^{\ddagger} = (D_{RX} + \lambda_0)/4$. [d] Experimental value.

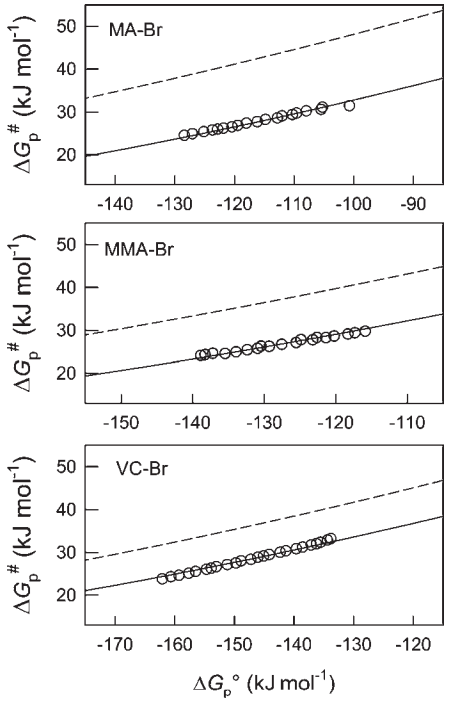

Figure 4. Variation of the activation free energy with the standard free energy of the reaction for the dissociative electron transfer to alkyl bromides in CH_3CN. The dashed and solid lines are the predictions of the classical and "sticky" dissociative electron transfer models, respectively.

where the collision frequency, Z^{el}, is the collision number at the electrode, which can be estimated by eq 7:[43]

$$Z^{el} = (RT/2\pi M)^{1/2} \quad (7)$$

in which M is the molar mass. The diffusion coefficient, D, of the reactant RX can be calculated from the voltammetric peak current.[40] The calculated values of Z^{el} and D, together with the voltammeric data, are summarized in Table 2.

At the peak potential, the standard free energy of the reaction is given by the difference between E_p and the standard reduction potential of RX, $E^o_{RX/R^\bullet+X^-}$. However, the latter cannot be measured experimentally because of the irreversibility of the dissociative electron transfer to RX. It can be estimated by considering a homolytic dissociation of RX followed by 1e$^-$ reduction of X$^\bullet$ to X$^-$, both reactions occurring in the desired solvent (CH_3CN in our case). Accordingly, $E^o_{RX/R^\bullet+X^-}$ can be expressed as[44]

$$E^\circ_{RX/R^\bullet+X^-} = E^\circ_{X^\bullet/X^-} - \frac{\Delta_{BD}G^\circ}{F} \quad (8)$$

where $E^o_{X^\bullet/X^-}$ is the standard reduction potential of X$^\bullet$, and $\Delta_{BD}G^o$ is the free energy of the homolytic bond dissociation. $E^o_{Br^\bullet/Br^-}$ in CH_3CN has recently been estimated from thermochemical data to be 1.60 V vs SCE.[44] Experimental data for the bond dissociation energy are not available. However, theoretically computed $\Delta_{BD}G^o$ values based on high-level ab initio molecular orbital calculations in CH_3CN are available for all three compounds.[14] We used these values and the resulting standard reduction potentials calculated from eq 8 are listed in Table 3, together with the literature values of D_{RBr} and $\Delta_{BD}G^o$.

Using the experimental α, D, and E_p values, a series of $\Delta G_p^{\ddagger}$ values was calculated from eq 6 for a wide range of scan rates. The corresponding free energy of the ET reaction was calculated for each scan rate as $\Delta G_p^o = F(E_p - E^o_{RX/R^\bullet+X^-})$. The last term needed to apply eq 5 is the solvent reorganization energy λ_o. This can be estimated from eq 9, using the radii (a) of spheres equivalent to RX molecules:[43,45]

$$\lambda_o(\text{eV}) = \frac{3}{a\ (\text{Å})} \quad (9)$$

This equation has been derived from experimental data for dimethylformamide, but we assume it to be approximately valid also for CH_3CN. The equivalent radii were calculated from eq 10:[15b]

$$a = \frac{(2a_{RBr} - a_{Br^-})a_{Br^-}}{a_{RBr}} \quad (10)$$

The RBr molecular radius, a_{RBr}, can be calculated from the density (ρ) and molecular mass of RX according to eq 11,[43] whereas a_{Br^-} = 1.96 Å is from crystallographic data.[46]

$$a = \left(\frac{3M}{4N_A\pi\rho}\right)^{1/3} \quad (11)$$

The equivalent molecular radii and the solvent reorganization energies calculated for the three alkyl bromides are listed in Table 3. The reported values of λ_o can be used, together with the R-Br bond dissociation energies to calculate the intrinsic barrier, $\Delta G_0^{\ddagger} = (D_{RX} + \lambda_0)/4$, expected according to the classical version of the dissociative ET theory. These predicted values are included in Table 3.

Figure 4 shows a comparison of the experimental $\Delta G_p^{\ddagger}$ versus ΔG_p^o plots with predictions of eq 5 (dashed line). Application of the classical dissociative ET (eq 5) clearly does not give a satisfactory fitting of the experimental data, the predicted activation free energies being significantly greater than the experimental ones. This discrepancy is most likely due to in-cage ion−radical interactions between the ET product fragments R$^\bullet$ and Br$^-$.

Indeed, DFT calculations have shown the existence of weakly associated radical and anion pairs in the gas phase. We therefore

checked the applicability of the sticky dissociative ET model, which takes into account the possibility of fragment interactions in the solvent cage. The sticky model introduces the ion−dipole interaction energy, D_p, in the classical version of the dissociative ET theory, slightly modifying eq 5 as follows:[7]

$$\Delta G^{\ddagger} = \frac{(\sqrt{D_{RX}} - \sqrt{D_P})^2 + \lambda_o}{4}\left(1 + \frac{\Delta G^{\circ} - D_p}{(\sqrt{D_{RX}} - \sqrt{D_P})^2 + \lambda_o}\right)^2 \quad (12)$$

As shown in eq 12, D_p modifies not only the driving force of the reaction but also decreases the intrinsic barrier. Thus, a quite small value of D_p may result in a significant modification of the kinetics of the dissociative ET.[8,9]

Using D_p as the only adjustable parameter, we fitted the experimental $\Delta G_p^{\ddagger}$ versus ΔG_p^{o} plots to eq 12. As shown in Figure 4, an excellent fit is achieved for all three alkyl bromides and the best fitting D_p values are reported in Table 3. Reported also in the table are the intrinsic barriers calculated from the sticky model: $\Delta G_0^{\ddagger} = [((D_{RX})^{1/2} - (D_p)^{1/2})^2 + \lambda_0]/4$.

The above-described experimental results agree very well with the theoretical calculations, showing that electron transfer to RX does not produce $RX^{\bullet -}$ but only loose ion−radical complexes ($R^{\bullet}\cdots X^{-}$). As a matter of fact, there is a slight divergence between experiment and theory. The theoretical calculations show the presence of loose complexes in the gas phase but not in solution, whereas the experimental results confirm the sticky model for all three alkyl halides. This divergence of theory[14] from experiment[8,9] has already been observed for other systems and is most likely due to a failure of the currently employed computational solvation models to observe such weakly interacting adducts. In essence, the stabilization energy of these complexes is within the typical uncertainty of the calculated solvation energies (ca. 1−2 kcal mol^{-1}).

A further support of the sticky DET mechanism evidenced by the CV studies may be obtained by comparing the experimentally measured free energies of activation, $\Delta G^{\ddagger}$, with data from theoretical computations. To this end, we performed multireference calculations to determine the potential energy surfaces and activation barriers of the reductive cleavage of MA-Br, MMA-Br, and VC-Br according to the following reactions:

$$RBr_{(g)} + e^{-}{}_{(g)} \rightarrow R^{\bullet}{}_{(g)} + Br^{-}{}_{(g)} \quad (13)$$

$$RBr_{(sol)} + e^{-}{}_{(g)} \rightarrow R^{\bullet}{}_{(sol)} + Br^{-}{}_{(sol)} \quad (14)$$

where the subscript (sol) stands for the solution phase (acetonitrile in this case). Examples of the calculated energy profiles as a function of the C−X bond distance are reported in Figure 5 for MA-Br. Comparing the energy profiles in the gas phase with those in acetonitrile shows that the energy curve for the anionic species shifts to lower values because of solvation, whereas that of RX is little affected. The activation energy for the DET can be estimated from the crossing point between the two potential energy profiles. However, to obtain meaningful data that are comparable with the experimental results, one has to take the electrode potential into account in the calculation of the potential energy surfaces. This can be done by assuming that the electrode potential affects only the energy profile of the reagents ($RX + e^{-}$).[40] The contribution of the electrode potential E_{elec} to the overall energy of the reagents is given by $\Delta G = -FE_{elec}$. However, before we do this conversion, we have to change the electrode potential, which is a relative value measured

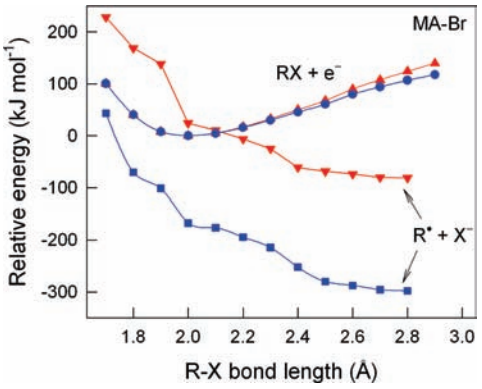

Figure 5. Relative positions of the potential energy surfaces for the reductive cleavage of MA-Br calculated in the gas (red) and solution (blue) phases. MRMP2/6-31+G(d)//MCSCF/6-31+G(d) and MRMP2/6-31+G(d)//MCSCF/6-31+G(d) + PCM/UAHF were used for the gas- and solution-phase calculations, respectively.

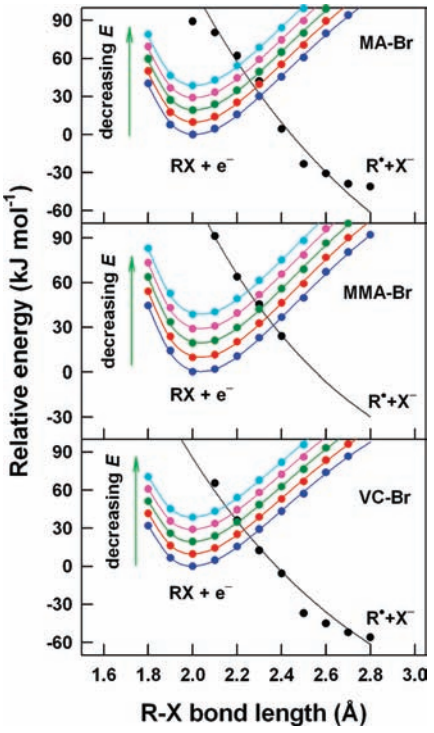

Figure 6. Profiles of the potential energy surfaces calculated for the dissociative electron transfer to MA-Br, MMA-Br, and VC-Br. All calculations are based on MRMP2/6-31+G(d)//MCSCF/6-31+G(d) + PCM/UAHF with correction of the relative position of the potential energy surface of the reagents for the electrode potential.

in acetonitrile with respect to aqueous calomel electrode (E^{SCE}_{elec,CH_3CN}), to an absolute value (E^{abs}_{elec,CH_3CN}). An expression allowing conversion of relative potentials in acetonitrile to absolute values has recently been reported.[47] Using that expression leads to the following equation for the conversion of E^{SCE}_{elec,CH_3CN} to E^{abs}_{elec,CH_3CN}:

$$E^{abs}_{elec,CH_3CN} = E^{SCE}_{elec,CH_3CN} + 4.429V \quad (15)$$

Figure 6 shows the potential energy profiles calculated in acetonitrile for the reductive cleavage of each alkyl halide at different potentials. Calculations were made for each RX by

dx.doi.org/10.1021/ja110538b | J. Am. Chem. Soc. 2011, 133, 6254–6264

Table 4. Kinetic and Thermodynamic Parameters of Relevance in the Analysis of Dissociative ET to Some Alkyl Bromides in CH_3CN

	E_p,[a] V vs SCE	$E^o_{RX/R^{\bullet}+X^-}$,[b] V vs SCE	$FE^{o,abs}_{RX/R^{\bullet}+X^-}$, kJ/mol	ΔG^o_p, kJ/mol	$\Delta G^{\ddagger(theory)}_p$,[c] kJ/mol	$\Delta G^{\ddagger(exptl)}_p$,[d] kJ/mol
MA-Br	−1.77	−0.68	256.56	−105.2	30.7	30.8
MMA-Br	−1.78	−0.64	255.59	−110.0	31.3	31.1
VC-Br	−2.28	−0.83	207.35	−139.9	22.9	30.9

[a] At v = 0.2 V s^{-1}. [b] Taken from ref 44. [c] Theoretically computed values. [d] Experimental data.

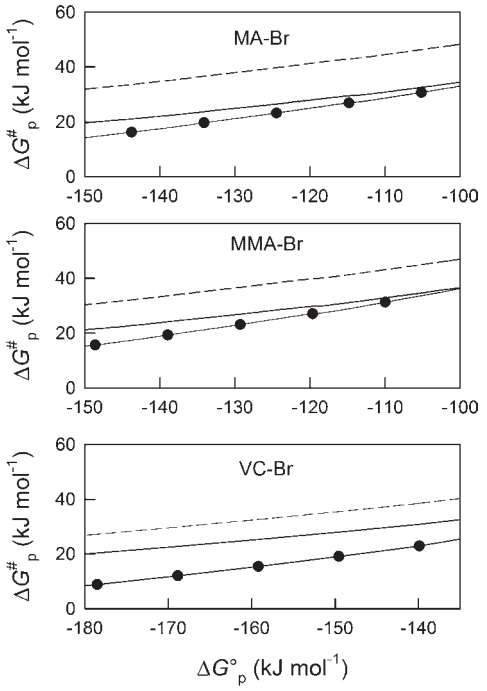

Figure 7. Variation of the activation free energy as a function of the standard reaction free energy for the dissociative electron transfer to alkyl bromides in MeCN. Comparison between theory (●), experiment (—), and predictions of the classical ET model (− −). MRMP2/6-31+G(d)//MCSCF/6-31+G(d) + PCM/UAHF are used in all calculations.

decreasing the electrode potential by 0.1 V, starting from −1.77, −1.78, and −2.28 for MA-Br, MMA-Br, and VC-Br, respectively. The range of electrode potential was chosen so that a set of data falling within the range of the experimental measurements could be computed for each compound. These energy profiles can now be used to estimate the activation free energy of the process as a function of the applied potential. To make easier determination of the crossing points, the energy profiles calculated for the reagents were fitted to the R−X Morse curve, whereas as those of the products were fitted to the repulsive part of the Morse curve.[41] This gives the curves shown in Figure 6, which have been used to calculate the activation free energies. As can be seen $\Delta G^{\ddagger}$ decreases as the electrode potential becomes more negative in accord with the well-known dependence of electron transfer rate constant on potential. In Table 4, we report theoretically calculated $\Delta G^{\ddagger}$ values obtained at electrode potentials corresponding to the peak potentials measured at v = 0.2 V s^{-1}, and these values generally compare very well with the activation free energies calculated from the CV data at the same scan rate.

In Figure 7 the dependence of the calculated activation free energy on the standard reaction free energy is reported. For the sake of comparison, the figure also reports the experimental data, which are well described by the sticky model (see Figure 4), as well as those predicted according to the classical concerted electron transfer theory. We can observe a very good agreement between the computed and experimental results, except in the case of VC-Br. The slight disagreement between theory and experiment observed for VC-Br is probably due to certain constraints used during the calculations. In particular, the radical anion of VC-Br has an additional bond constraint (C−Cl bond length = 1.794517 Å), which was introduced to avoid detachment of the Cl atom during energy optimization.

■ CONCLUSIONS AND IMPLICATIONS

It is clearly shown, using both experimental and quantum-chemically calculated data, that dissociative electron transfer to some activated alkyl halides, typical of those commonly used as initiators in living radical polymerization (LRP), does not produce intermediate radical anions. Reductive cleavage of these compounds follows a concerted mechanism in which electron transfer and bond breaking occur in a single step. This is true also for other alkyl halides of relevance to LRP such as haloacetonitriles,[14,9] benzyl halides,[15b] and polyhalomethanes.[8b] This finding is of crucial importance for a full understanding of the mechanism of RX activation by copper catalysts. Activation of RX by Cu^0 in SET-LRP was originally proposed to occur by an outer-sphere electron transfer involving the intermediate formation of $RX^{\bullet-}$.[31] However, in light of the results reported herein, any mechanistic interpretation for SET-LRP or ATRP involving $RX^{\bullet-}$ should be discarded. If OSET really occurs in these processes, it has to follow a concerted DET mechanism. Since, however, concerted DET to a C−X bond is characterized by a high intrinsic barrier, $\Delta G^{\ddagger}_0$, mainly due to a contribution from the breaking bond, the process can proceed to a reasonable rate only with OSET donors having highly negative potentials. Of course, this is not the case of the copper complexes (E^o > −0.6 V vs SCE)[48] or metallic copper used as activators in ATRP and SET-LRP. These catalysts follow a different mechanism in which the high $\Delta G^{\ddagger}$ involved in concerted DET is avoided by favorable interactions between RX and the catalyst leading to a bonded transition state with low activation free energy (ISET-AT mechanism). On the other hand, an OSET donor could hardly function as a good catalyst of a LRP based on the activation of C−X bonds because its redox potential should be so negative that the propagating radicals would also be rapidly reduced to the corresponding carbanions.[38] Thus, a good catalyst for LRP must be able to react with both the initiator R−X and the dormant species P_n−X through an ISET-AT mechanism.

A second important outcome of this study is the inappropriateness of using homolytic or heterolytic bond dissociation as a means of classifying metal-catalyzed LRP. On the basis of quantum-chemically calculated data, C−X bond dissociation during the activation step of SET-LRP cannot be classified as

either being homolytic or heterolytic because injection of one electron in RX produces an ion−radical adduct without a covalent bond between carbon and the bromide anion. In contrast, if activation of RX by Cu^I complexes in ATRP occurs via atom transfer, the process may be considered as a metal-catalyzed homolytic C−X bond dissociation. In our opinion, however, the classification of the LRP techniques based on the C−X bond dissociation mechanism (X = ONR_2 in NMP; SC(S)R in RAFT; Cl, Br, or I in ATRP and SET-LRP, etc.) is confusing because focusing primarily on the mode of C−X bond cleavage (homolytic, heterolytic), which as we have shown is not always possible, one can have difficulty while classifying the LRP systems because different mechanisms may involve the same mode of C−X bond dissociation. In addition, the determination of the precise mechanism of the C−X bond cleavage requires extensive theoretical and/or experimental efforts as demonstrated in this work.

A third very important conclusion can be drawn from the comparison of the experimental activation free energies with theoretically computed values. This is the first report of such a comparison, which shows a close agreement between theory and experiment. The computed potential energy surfaces of the separating radical and halide anion are, of course, a reliable evaluation of all the interactions between the two fragments. The agreement with experimental data, which fit very well the sticky model, is a relevant support for the appropriateness of this simplified model, which considers only the ion−dipole interactions.

■ ASSOCIATED CONTENT

Supporting Information. Full computational results, including Gaussian archive entries for the optimized geometries of the calculated species and complete ref 33a. This material is available free of charge via the Internet at http://pubs.acs.org.

■ AUTHOR INFORMATION

Corresponding Author
armando.gennaro@unipd.it;
mcoote@rsc.anu.edu.au;
tamaz.guliashvili@ge.com

■ ACKNOWLEDGMENT

T.G. gratefully acknowledges GE Water & Process Technologies for support, M.L.C., C.Y.L., and J.L.H. gratefully acknowledge generous allocations of computing time under the Merit Allocation Scheme and Partner-Share Scheme on the NCI National Facility at the Australian National University, and support from the Australian Research Council under their Centres of Excellence program. A.A.I. and A.G. gratefully acknowledge support by the University of Padova through grant CPDA083370.

■ REFERENCES

(1) Wang, J.-S.; Matyjaszewski, K. *J. Am. Chem. Soc.* **1995**, *117*, 5614–5615.
(2) Kato, M.; Kamigaito, M.; Sawamoto, M.; Higashimura, T. *Macromolecules* **1995**, *28*, 1721–1723.
(3) Xia, J.; Matyjaszewski, K. *Chem. Rev.* **2001**, *101*, 2921–2990.
(4) Kamigaito, M.; Ando, T.; Sawamoto, M. *Chem. Rev.* **2001**, *101*, 3689–3745.
(5) (a) Tsarevsky, N. V.; Matyjaszewski, K. *Chem. Rev.* **2007**, *107*, 2270–2299. (b) Matyjaszewski, K.; Tsarevsky, N. V. *Nat. Chem.* **2009**, *1*, 276–288.
(6) Fischer, H. *Chem. Rev.* **2001**, *101*, 3581–3610.
(7) Costentin, C.; Robert, M.; Savéant, J.-M. *Chem. Phys.* **2006**, *324*, 40–56.
(8) (a) Pause, L.; Robert, M.; Savéant, J.-M. *J. Am. Chem. Soc.* **2000**, *122*, 9829–9835. (b) Costentin, C.; Robert, M.; Savéant, J.-M. *J. Am. Chem. Soc.* **2003**, *125*, 10729–10739. (c) Costentin, C.; Louault, C.; Robert, M.; Teillout, A.-L. *J. Phys. Chem. A* **2005**, *109*, 2984–2990.
(9) (a) Cardinale, A.; Isse, A. A.; Gennaro, A.; Robert, M.; Savéant, J.-M. *J. Am. Chem. Soc.* **2002**, *124*, 13533–13539. (b) Isse, A. A.; Gennaro, A. *J. Phys. Chem. A* **2004**, *108*, 4180–4186.
(10) Pause, L.; Robert, M.; Savéant, J.-M. *J. Am. Chem. Soc.* **2001**, *123*, 11908–11916.
(11) Tikhomirov, V. A.; German, E. D; Kuznetsov, A. M. *Chem. Phys.* **1995**, *191*, 25–30.
(12) (a) Takeda, N.; Poliakov, P. V.; Cook, A. R.; Miller, J. R. *J. Am. Chem. Soc.* **2004**, *126*, 4301–4309. (b) Costentin, C.; Robert, M.; Savéant, J.-M. *J. Am. Chem. Soc.* **2004**, *126*, 16834–16840.
(13) Rosen, B. M.; Percec, V. *J. Polym. Sci., Part A: Polym. Chem.* **2008**, *46*, 5633–5697.
(14) Lin, C. Y.; Coote, M. L.; Gennaro, A.; Matyjaszewski, K. *J. Am. Chem. Soc.* **2008**, *130*, 12762–12774.
(15) (a) Andrieux, C. P.; Gallardo, I.; Savéant, J.-M.; Su, K. B. *J. Am. Chem. Soc.* **1986**, *108*, 638–647. (b) Andrieux, C. P.; Le Gorande, A.; Savéant, J.-M. *J. Am. Chem. Soc.* **1992**, *114*, 6892–6904. (c) Pause, L.; Robert, M.; Savéant, J.-M. *J. Am. Chem. Soc.* **1999**, *121*, 7158–7159. (d) Isse, A. A.; Gottardello, S.; Durante, C.; Gennaro, A. *Phys. Chem. Chem. Phys.* **2008**, *10*, 2409–2416.
(16) (a) Andrieux, C. P.; Blocman, C.; Dumas-Bouchiat, J.-M.; Savéant, J.-M. *J. Am. Chem. Soc.* **1979**, *101*, 3431–3441. (b) Wipf, D. O.; Wightman, R. M. *J. Phys. Chem.* **1989**, *93*, 4286–4291. (c) Isse, A. A.; Mussini, P. R.; Gennaro, A. *J. Phys. Chem. C* **2009**, *113*, 14893–14992.
(17) (a) Savéant, J.-M. *J. Phys. Chem.* **1994**, *98*, 3716–3724. (b) Costentin, C.; Robert, M.; Savéant, J.-M. *J. Am. Chem. Soc.* **2004**, *126*, 16051–16057.
(18) (a) Andrieux, C. P.; Savéant, J.-M.; Tallec, A.; Tardival, R.; Tardy, C. *J. Am. Chem. Soc.* **1997**, *119*, 2420–2429. (b) Rossi, R. A.; Pierini, A. B.; Penényory, A. B. *Chem. Rev.* **2003**, *103*, 71–167.
(19) Matyjaszewski, K. *Macromolecules* **1998**, *31*, 4710–4717.
(20) Matyjaszewski, K. *Macromolecules* **2002**, *35*, 6773–6781.
(21) Singleton, D. A.; Nowlan, D. T., III; Jahed, N.; Matyjaszewski, K. *Macromolecules* **2003**, *36*, 8609–8616.
(22) Pintauer, T.; Zhou, P.; Matyjaszewski, K. *J. Am. Chem. Soc.* **2002**, *124*, 8196–8197.
(23) Pintauer, T.; Braunecker, W. A.; Collange, E.; Poli, R.; Matyjaszewski, K. *Macromolecules* **2004**, *34*, 2679–2682.
(24) Tang, W.; Matyjaszewski, K. *Macromolecules* **2007**, *40*, 1858–1863.
(25) Tang, W.; Kwak, Y.; Braunecker, W. A.; Tsarevsky, N.; Coote, M. L.; Matyjaszewski, K. *J. Am. Chem. Soc.* **2008**, *130*, 10702–10713.
(26) Tsarevsky, N. V.; Braunecker, W. A.; Matyjaszewski, K. *J. Organomet. Chem.* **2007**, *692*, 3212–3222.
(27) Tsarevsky, N. V.; Braunecker, W. A.; Vacca, A.; Gans, P.; Matyjaszewski, K. *Macromol. Symp.* **2007**, *248*, 60–70.
(28) Percec, V.; Guliashvili, T.; Ladislaw, J. S.; Wistrand, A.; Stjerndahl, A.; Sienkowska, M. J.; Monteiro, M. J.; Sahoo, S. J. *J. Am. Chem. Soc.* **2006**, *128*, 14156.
(29) Guliashvili, T.; Percec, V. *J. Polym. Sci., Part A: Polym. Chem.* **2007**, *45*, 1607.
(30) Matyjaszewski, K.; Tsarevsky, N. V.; Braunecker, W. A.; Dong, H.; Huang, J.; Jakubowski, W.; Kwak, Y.; Nicolay, R.; Tang, W.; Yoon, J. A. *Macromolecules* **2007**, *40*, 7795–7806.
(31) Rosen, B. M.; Percec, V. *Chem. Rev.* **2009**, *109*, 5069–5119.
(32) (a) Matyjaszewski, K.; Coca, K.; Gaynor, S. G.; Mingli Wei, M.; Woodworth, B. E. *Macromolecules* **1997**, *30*, 7348–7350. (b) Matyjaszewski, K.; Pyun, J.; Gaynor, S. G. *Macromol. Rapid Commun.* **1998**, *19*, 665–670.

(33) (a) Frisch, M. J.; et al. *Gaussian 03, Revision B.03*; Gaussian, Inc.: Pittsburgh PA, 2003.(b) Schmidt, M. W.; Baldridge, K. K.; Boatz, J. A.; Elbert, S. T.; Gordon, M. S.; Jensen, J. H.; Koseki, S.; Matsunaga, N.; Nguyen, K. A.; Su, S. J.; Windus, T. L.; Dupuis, M.; Montgomery, J. A. *J. Comput. Chem.* **1993**, *14*, 1347–1363. (c) Bode, B. M.; Gorden, M. S. *J. Mol. Graphics Model.* **1998**, *16*, 133–138.

(34) Ruiz, E.; Cirera, J.; Alvarez, S. *Coord. Chem. Rev.* **2005**, *249*, 2649–2660 and references cited therein.

(35) Maslak, P.; McGuinn, J. M. *Chem. Commun.* **1999**, 2467–2468.

(36) Hansch, C.; Leo, A.; Taft, W. R. *Chem. Rev.* **1991**, *91*, 165–195.

(37) Sienkowska, M. J.; Rosen, B. M.; Percec, V. *J. Polym. Sci., Part A: Polym. Chem.* **2009**, *47*, 4130–4140.

(38) Bortolamei, N.; Isse, A. A.; Gennaro, A. *Electrochim. Acta* **2010**, *55*, 8312–8318.

(39) (a) Isse, A. A.; Abdurahman, A. M.; Vianello, E. *J. Chem. Soc., Perkins Trans 2* **1996**, 597–600. (b) Isse, A. A.; Gennaro, A.; Vianello, E. *Electrochim. Acta* **1997**, *42*, 2065–2071.

(40) Bard, A. J.; Faulkner, L. R. *Electrochemical Methods*, 2nd ed.; John Wiley & Sons: New York, 2001.

(41) (a) Savéant, J.-M. *Elements of Molecular and Biomolecular Electrochemistry*; Wiley-Interscience: New York, 2006. (b) Savéant, J.-M. *J. Am. Chem. Soc.* **1987**, *109*, 6788–6795.

(42) Savéant, J.-M. *J. Phys. Chem. B* **2002**, *106*, 9387–9395.

(43) Kojima, H.; Bard, A. J. *J. Am. Chem. Soc.* **1975**, *97*, 6317–6324.

(44) Isse, A. A.; Lin, C. Y.; Coote, M. L.; Gennaro, A. *J. Phys. Chem. B* **2011**, *115*, 678–684.

(45) Andrieux, C. P.; Savéant, J.-M.; Tardy, C. *J. Am. Chem. Soc.* **1998**, *120*, 4167–4175.

(46) Lide, D. R., Ed. *CRC Handbook of Chemistry and Physics*, 87th ed., Taylor and Francis: Boca Raton, FL, 2007.

(47) Isse, A. A.; Gennaro, A. *J. Phys. Chem. B* **2010**, *114*, 7894–7899.

(48) (a) Qiu, J.; Matyjaszewski, K.; Thouin, L.; Amatore, C. *Macromol. Chem. Phys.* **2000**, *201*, 1625–1631. (b) Coullerez, G.; Malmström, E.; Jonsson, M. *J. Phys. Chem. A* **2006**, *110*, 10355–10360. (c) Tsarevsky, N. V.; Braunecker, W. A.; Tang, W.; Brooks, S. J.; Matyjaszewski, K.; Weisman, G. R.; Wong, E. H. *J. Mol. Catal. A: Chem.* **2006**, *257*, 132–140.

NOTE ADDED AFTER ASAP PUBLICATION

Due to production error, the version of this paper that was published online February 7, 2011, was missing several text corrections. The revised version was published February 18, 2011.